Waveform inversion for D″ structure beneath northern Asia using Hi-net tiltmeter data

Kenji Kawai,[1,2] Shutaro Sekine,[3] Nobuaki Fuji,[4] and Robert J. Geller[4]

K. Kawai, Department of Earth and Planetary Sciences, Tokyo Institute of Technology, Ookayama 2-12-1, Meguro-ku, Tokyo, 152-8551, Japan. (kenji@geo.titech.ac.jp)

Institut de Physique du Globe de Paris, 4 Place Jussieu-75252, Paris Cedex 05, France.

R.J. Geller and N. Fuji, Department of Earth and Planetary Science, Graduate School of Science, Tokyo University, Hongo 7-3-1, Bunkyo-ku, Tokyo, 113-0033, Japan. ([bob,fuji]@eps.s.u-tokyo.ac.jp)

S. Sekine, National Research Institute for Earth Science and Disaster Prevention, Tennodai 3-1, Tsukuba, Ibaraki, 305-0006, Japan. (ssekine@bosai.go.jp)

[1]Department of Earth and Planetary

We invert shear-wave waveform data for the radial variation of (isotropic) shear-velocity in D″ beneath Northern Asia. We reduce source and receiver effects by using data for intermediate and deep events beneath Italy and Japan recorded respectively at stations in East Asia and Europe. Relative to PREM, we find a significantly higher S-wave velocity in the depth range from 150 to 300 km above the core-mantle boundary (CMB) and a slightly lower S-wave velocity in the depth range 0-150 km above the CMB. As our previous studies of D″ structure beneath Central America and the Arctic obtained similar S-wave velocity models, we suggest that this pattern of vertical dependence of shear wave velocity in D″ may be a general phenomenon, at least in relatively cold regions.

Sciences, Tokyo Institute of Technology,
Tokyo, Japan.

[2]Institut de Physique du Globe de Paris,
Paris, France

[3]National Research Institute for Earth
Science and Disaster Prevention, Tsukuba,
Ibaraki, Japan.

[4]Department of Earth and Planetary
Science, Graduate School of Science, Tokyo
University, Tokyo, Japan.

1. Introduction

The lowermost mantle, which is known as D″, plays a crucial role in the Earth's deep interior. D″ is both a thermal and a chemical boundary layer between the mantle and the outer core. The top of D″ is now generally explained as the phase transition from perovskite (pv) to post-perovskite (ppv) [*Murakami et al.*, 2004]. Although the top of D″ is now thought to be well understood, seismic structure within D″ remains an important issue.

We have developed methods for waveform inversion for localized structure [*Geller and Hara*, 1993; *Kawai et al.*, 2006, 2007a]. Using these methods, *Kawai et al.* [2007a] analyzed waveform data of events beneath South America observed in Western North America and found a high S-velocity (relative to PREM) in the upper half of D″ and almost the same velocity as PREM in the lower half of D″. *Kawai et al.* [2007b] found a similar velocity structure under the Arctic. On the other hand, we found a more complex "S-shaped" model beneath the western Pacific whose average velocity is slow [*Konishi et al.*, 2009]. The "S-shaped" model suggests a large presence of subducted MORB beneath the western Pacific, which is consistent with the expected existence of a "slab-graveyard" there [*Maruyama et al.*, 2007].

Many studies of mantle tomography have suggested that high-velocity regions can be interpreted as low temperature regions (e.g., beneath Central America [e.g. *Megnin and Romanowicz*, 2000]). In order to further investigate D″ structure in such regions, we study the S-wave velocity structure of the lowermost mantle beneath Northern Asia in this paper.

2. Target region and waveform data

A highly dense and sensitive short period network (Hi-net) has been deployed in Japan by the National Research Institute for Earth Science and Disaster Prevention (NIED). NIED also has deployed high sensitivity accelerometers (i.e., tiltmeters) in the same boreholes as the short period sensors [*Obara et al.*, 2005]. The tiltmeters can be used as broadband seismometers in the frequency band between 0.02 and 0.16 Hz [*Tonegawa et al.*, 2006]. Although the tiltmeters record only horizontal motions, the Hi-net tiltmeter network is currently the densest broadband array in the world. This is the first study in which Hi-net data are used to conduct waveform inversion.

We study the D″ layer beneath Northern Asia (Fig. 1). We use waveforms from 2 intermediate-depth earthquakes under Italy (I-events) and 17 intermediate-depth and deep earthquakes under Japan and East Asia (J-events) recorded by Hi-net tiltmeters and also by broadband seismometers from the global network (Table 1).

We use the transverse components of waveform data (obtained by rotating the N-S and E-W components) for 19 events (Table 1; Fig. 1). We apply a bandpass filter to the tiltmeter data and the broadband data and construct datasets for the passbands 0.02 to 0.05 Hz and 0.005 to 0.05 Hz (i.e., for the period ranges, 20-50 s and 20-200 s), respectively. In this study we use earthquakes whose source time function can be approximated as a δ-function at the centroid time for the frequency band used in the data analysis.

The broadband data are processed in the same way as *Kawai et al.* [2007a], except that we use broadband velocity data, so the tiltmeter data must be integrated. The integrated tiltmeter data are almost identical to the F-net wave data at periods between

6 s and 50 s. We rotate the waveform data according to the estimated azimuth of the Hi-net borehole sensors compared to the NIED F-net [*Shiomi et al.*, 2003]. The tiltmeter data are in units of tilt angle (in radians) for the N-S and E-W directions. We obtain horizontal accelerations by multiplying the tilt angles by $-g$, where g is the gravitational acceleration. Next, we integrate the data from acceleration to velocity after applying a high-pass filter with a corner at 0.01 Hz to avoid instability in integration. Finally, we apply a bandpass filter to the data and construct datasets for the passband from 0.02 to 0.05 Hz. The synthetics are processed in the same way as the data.

We select time windows which include the S and ScS phases from the transverse component. We use the same selection criteria for data quality as *Kawai et al.* [2007a]. We choose a dataset of 906 time windows that satisfy the criteria (We reject the remaining 1992 windows.) out of a total of 2898 time windows. The reciprocal of the maximum amplitude in each time window is used as the weighting factor in the inversion for the J-events and that factor is further multiplied by a factor of 1/50 for the I-events, so that each event has roughly the same importance. The factor of 1/50 is needed because the number of data for I-events is very large (more than 500 stations) and the range of epicentral distances is very narrow (all of the Hi-net stations are at distances between 83° and 92° for event I2).

Since the inversion is only for the structure of D″ in the target region, other effects must be accounted for empirically. To correct for the effect of local structure near the stations and the sources, we make "static" corrections using the time shift which gives the best

correlation coefficient between the synthetic and observed seismograms. As the inversion is conducted in the same manner as *Konishi et al.* [2009], details are omitted here.

3. Inversion results

The initial model is anisotropic PREM [*Dziewonski and Anderson*, 1981]. The source parameters (moment tensors and centroids) are fixed to the Global CMT solution. We conduct inversions using the eigenvectors corresponding to the n largest eigenvalues of the singular value decomposition (SVD) of the matrix of partial derivatives as the basis functions for the perturbation to the starting model yielding models SVD2 and SVD3 for $n = 2$ and $n = 3$ respectively. In order to examine the robustness of the inversion results, we vary the 'tie-in depth,' the depth above which the model is fixed to the initial model (PREM). We invert respectively for tie-in depths of 260, 280, 300, 320, and 340 km above the CMB. Ten similar models are obtained (Fig. 2).

Table 2 shows the variance data and Akaike Information Criterion (AIC) [*Akaike*, 1977] value for each model. AIC rewards variance reduction and penalizes increases in the number of model parameters. Lower values of AIC denote models which are formally better, in a statistical sense. Defining the variance of the data to be 100 %, the variance of the residuals for PREM (the initial model), defined to be (data − PREM synthetics), is 104.6 %. Note that the variance values in Table 2 are obtained by using the Born approximation rather than by relinearizing with respect to the model obtained by the inversion. After making the static time shift the variance for (PREM with time shift) is reduced to 68.0 %. The residuals and AIC values for the ten models obtained by the SVD inversions are shown in Table 2. The variance values for all ten SVD models (64.2

%–62.1 %) are lower than that for (PREM with time shift, 68.0 %) while the AIC values (8909–9034) for the ten SVD models are lower than that for (PREM with time shift, 9247). This demonstrates the statistical significance of the ten SVD models.

All ten SVD models in Fig. 2a show high S-wave velocity in D″ (relative to PREM) in the zone from 200-300 km above the core-mantle boundary and slightly low velocity (relative to PREM) in the zone from 0-100 km above the CMB. Fig. 2b shows nominal error estimates made by treating the ten models in Fig. 2a as independent. The difference between the average of the ten SVD models and PREM is considerably greater than the nominal standard deviation, further supporting the statistical significance of the SVD models.

Ideally it would be possible to look at the observed waveforms for individual stations, and compare them to synthetics for PREM and for the final model to see visually as well as quantitatively the improvement in the fit. Unfortunately, however, the noise level is too high to allow meaningful visual study of individual records. We therefore have prepared "quality control stacks," (QC stacks) some of which are shown in Fig. 3, for each of the events in this study. These stacks are not intended for use in obtaining the Earth model, but rather merely as a check to ensure that the inversion result is reasonable. The stacks are made by aligning the records (after station and source corrections) using the PREM arrival time and normalizing the maximum amplitude of each of the observed records to one. Because a non-causal filter (in the passband 20-200 s) is used, there are signals before time $t = 0$. The synthetics are processed using the same weighting factors as the corresponding observed record. Model SVD3(340 km) was used as the final model.

Because there is not enough space to show all 19 events in Fig 3 we show QC stacks for events I1 and I2, and for every third J event (J1, J4, J7, J10, J13, and J16). The QC stacks in Fig. 3 show that the synthetics for the final model are, overall, a clear improvement over the initial model, thereby confirming that the inversion has reached a reasonable result.

To further validate our models we conduct resolution tests (Fig. 4). We compute synthetics for the two starting models shown in Fig. 4 for the sources and stations in our actual inversion. We then use PREM as the starting model and conduct an inversion of the synthetic data. The two-layered perturbations (Fig. 4a) could be satisfactorily resolved by both inversions. The three-layered perturbations (Fig. 4b) could be largely resolved by SVD3, but not by SVD2. Based on these resolution tests, our methods have the power to resolve models of the type shown in Figs. 2a and 2b.

4. Discussion

Previous studies of D″ near our study region have suggested the possibility of laterally heterogeneous structure of D″ [*Thomas et al.*, 2004; *Chambers and Woodhouse*, 2006]. The lateral temperature variation in D″ beneath Northern Asia may also be large [*Maruyama et al.*, 2007]. Thus it is possible that our velocity model (Fig. 2) represents the spatial average of laterally heterogeneous structure in the study region. Arguments from mineral physics show that impurities in Mg-pv decrease the shear wave velocity [*Tsuchiya and Tsuchiya*, 2006]. For example, a 1 mol% increase in the amount of both aluminum and iron will cause a 0.30 % velocity decrease in Mg-pv or a 0.37 % velocity decrease in Mg-ppv. Hence, the difference between D″ beneath Central America and Northern Asia can

be interpreted as due to the amount of impurities in Mg-ppv beneath Northern Asia being 1.5 mol% larger than that beneath Central America, on the assumption that the ratio of aluminum and iron is the same for both regions.

The D″ model obtained by this study can be interpreted as a "double crossing" phase transition (a ppv → pv reverse transition occurring within D″ [*Hernlund et al.*, 2005]), although we cannot exclude thermal effects. Hence, more quantitative studies such as modeling of seismic velocity based on mineral physics [*Wookey et al.*, 2005] are required in order to determine whether the velocity reduction in the lower half of D″ is due to double crossing phase transition or thermal effects. We also obtained similar models for D″ beneath Central America and the Arctic in our earlier work [*Kawai et al.*, 2007a, b]. Our results for these three regions, taken together, suggest that such velocity structure beneath cold regions may be ubiquitous. If so, this would have important implications for mineral physics, temperature profile, convection and material transport in D″.

Acknowledgments. We thank Kei Hirose, Taku Tsuchiya, and Shigenori Maruyama for valuable discussions. We thank Thorne Lay for comments and suggestions on an earlier version of this paper. We also thank Takuto Maeda and the other members of the Hi-net Group for their instruction of how to use Hi-net data. Data were obtained from the NIED Hi-net, NIED F-net, IRIS, ORFEUS and OHP data servers. KK and NF are supported by JSPS Fellowships for Young Scientists.

References

Akaike, H. (1977), Extension of method of maximum likelihood and the Stein's problem, *Annals of the Institute of Statistical Mathematics, 29*, 153–164.

Chambers, K., and J. H. Woodhouse (2006), Transient D″ discontinuity revealed by seismic migration, *Geophys. Res. Lett.*, *33,* L17312, doi:10.1029/2006GL027043.

Dziewonski, A. M., and D. L. Anderson (1981), Preliminary reference Earth model, *Phys. Earth Planet. Inter.*, *25,* 297–356.

Geller, R. J., and T. Hara (1993), Two efficient algorithms for iterative linearized inversion of seismic waveform data, *Geophys. J. Int., 115,* 699-710.

Hernlund, J. W., C. Thomas, and P. J. Tackley (2005), A doubling of the post-perovskite phase boundary and structure of the Earth's lowermost mantle, *Nature*, *434,* 882–886.

Kawai, K., N. Takeuchi, and R. J. Geller (2006), Complete synthetic seismograms up to 2 Hz for transversely isotropic spherically symmetric media, *Geophys. J. Int.*, *164,* 411–424.

Kawai, K., N. Takeuchi, R. J. Geller, and N. Fuji (2007a), Possible evidence for a double crossing phase transition in D″ beneath Central America from inversion of seismic waveforms, *Geophys. Res. Lett.*, *34,* L09314, doi:10.1029/2007GL029642.

Kawai, K., R. J. Geller, and N. Fuji (2007b), D″ beneath the Arctic from inversion of shear waveforms, *Geophys. Res. Lett.*, *34,* L21305, doi:10.1029/2007GL031517.

Konishi, K., K. Kawai, R. J. Geller, and N. Fuji (2009), MORB in the lowermost mantle beneath the western Pacific: Evidence from waveform inversion, *Earth Planet. Sci. Lett.*, *278,* 219–225.

Maruyama, S., M. Santosh, and D. P. Zhao (2007), Superplume, supercontinent, and post-perovskite: Mantle dynamics and anti-plate tectonics on the core-mantle boundary, *Gondowana Res.*, *11,* 7–37.

Megnin, C., and B. Romanowicz (2000), The three-dimensional shear velocity structure of the mantle from the inversion of body, surface and higher-mode waveforms, *Geophys. J. Int., 143,* 709–728.

Murakami, M., K. Hirose, K. Kawamura, N. Sata, and Y. Ohishi (2004), Post-perovskite phase transition in $MgSiO_3$, *Science*, *304,* 855–858.

Obara, K., K. Kasahara, K. Hori, and Y. Okada (2005), A densely distributed high-sensitivity seismograph network in Japan: Hi-net by National Research Institute for Earht Science and Disaster Prevention, *Rev. Sci. Instrum.*, *76,* 021301, doi:10.1063/1.1854197.

Shiomi, K., K. Obara, S. Aoi, and K. Kasahara (2003), Estimation on the azimuth of the Hi-net and KiK-net borehole seismometers, *Zisin 2*, *56,* 99–110 (in Japanese).

Thomas, C, J.-M. Kendall, and J. Lowman (2004), Lower-mantle seismic discontinuities and the thermal morphology of subducted slabs, *Earth Planet. Sci. Lett.*, *225,* 105–113.

Tonegawa, T., K. Hirahara, T. Shibutani, and K. Shiomi (2006), Upper mantle imaging beneath the Japan Islands by Hi-net tiltmeter recordings, *Earth Planets Space*, *58,* 1007–1012.

Tsuchiya, T., and J. Tsuchiya (2006), Effect of impurity on the elasticity of perovskite and postperovskite: Velocity contrast across the postperovskite transition in $(Mg,Fe,Al)(Si,Al)O_3$, *Geophys. Res. Lett., 33,* L12S04, doi:10.1029/2006GL025706.

Wookey, J., S. Stackhouse, J.-M. Kendall, J. Brodholt, and G. D. Price (2005), Efficacy of the post-perovskite phase as an explanation for lowermost-mantle seismic properties. *Nature, 438,* 1004–1007.

Event #	Date (Y/M/D)	Latitude	Longitude	Depth	M_w
I1	2004/5/5	38.61°	14.75°	238.9	5.5
I2	2006/10/26	38.65°	15.41°	216.8	5.8
J1	2002/6/3	27.50°	139.86°	491.2	5.8
J2	2002/6/28	43.74°	130.45°	581.5	7.3
J3	2002/9/15	44.77°	130.04°	589.4	6.4
J4	2002/11/17	47.81°	146.45°	479.8	7.3
J5	2003/7/27	46.99°	139.23°	477.2	6.7
J6	2003/8/31	43.38°	132.37°	493.0	6.1
J7	2003/11/12	33.31°	137.09°	381.8	6.3
J8	2004/11/7	47.93°	144.52°	493.0	6.1
J9	2005/2/22	33.15°	137.16°	372.2	5.6
J10	2005/4/19	29.66°	139.03°	417.9	5.9
J11	2005/10/23	37.36°	134.61°	393.5	5.9
J12	2006/3/28	31.72°	137.79°	411.6	5.9
J13	2006/4/16	30.29°	138.60°	423.6	5.7
J14	2006/6/11	33.15°	131.34°	144.5	6.4
J15	2006/9/16	41.33°	135.71°	382.2	5.9
J16	2007/1/15	34.94°	138.81°	169.8	5.9
J17	2007/4/1	32.27°	137.64°	379.7	5.7

Table 1. Earthquakes used in this study.

Model	variance %	AIC
PREM	104.6	10870
PREM with time shift	68.0	9248
SVD2 (260 km)	64.2	9034
SVD3 (260 km)	63.8	9013
SVD2 (280 km)	63.7	9005
SVD3 (280 km)	63.4	8990
SVD2 (300 km)	63.2	8974
SVD3 (300 km)	63.0	8963
SVD2 (320 km)	62.7	8943
SVD3 (320 km)	62.5	8936
SVD2 (340 km)	62.2	8914
SVD3 (340 km)	62.1	8909

Table 2. Variance and AIC for each model.

Figure 1. Event-receiver geometry, with great circle ray paths. The portions of the great circles which sample D″ are shown in red. Blue reversed triangles and red stars show the sites of stations used in our study and earthquakes studied, respectively. Plus signs are the bounce points indicated by geometrical optics.

Figure 2. (a) SVD inversions with 2 and 3 basis functions for tie-in depths of 340, 320, 300, 280, and 260 km, respectively. The parameters obtained by the inversions vary somewhat, but the same basic features (higher S-velocity, relative to PREM, in the upper half of D″, and lower S-velocity, relative to PREM, in the lower half) are found by all of the SVD inversions. (b) The average of the ten SVD models shown in Fig. 2a. The error bar is one standard deviation, treating the ten SVD models as independent.

Figure 3. "Quality control stacks," computed as follows. First all of the observed waveforms for each event which met the selection criteria were time shifted using PREM, after making the same source and station corrections as in the inversion. These waveforms were then filtered in the passband 20 s to 200 s using a four-pole non-causal bandpass filter. The maximum amplitude of each observed record was normalized to one, and the waveforms were then stacked (thick curves). The synthetics for the initial model (PREM, dotted curves) and final model (thin solid curves) were stacked using the same weighting factors as for the corresponding observed record. Model SVD3(340 km) was used as the final model.

Figure 4. Resolution test for D″ structure. Our methods and present dataset can successfully resolve the two-layered models (a). The details of the three-layered models were partially resolved by SVD3, but not by SVD2.

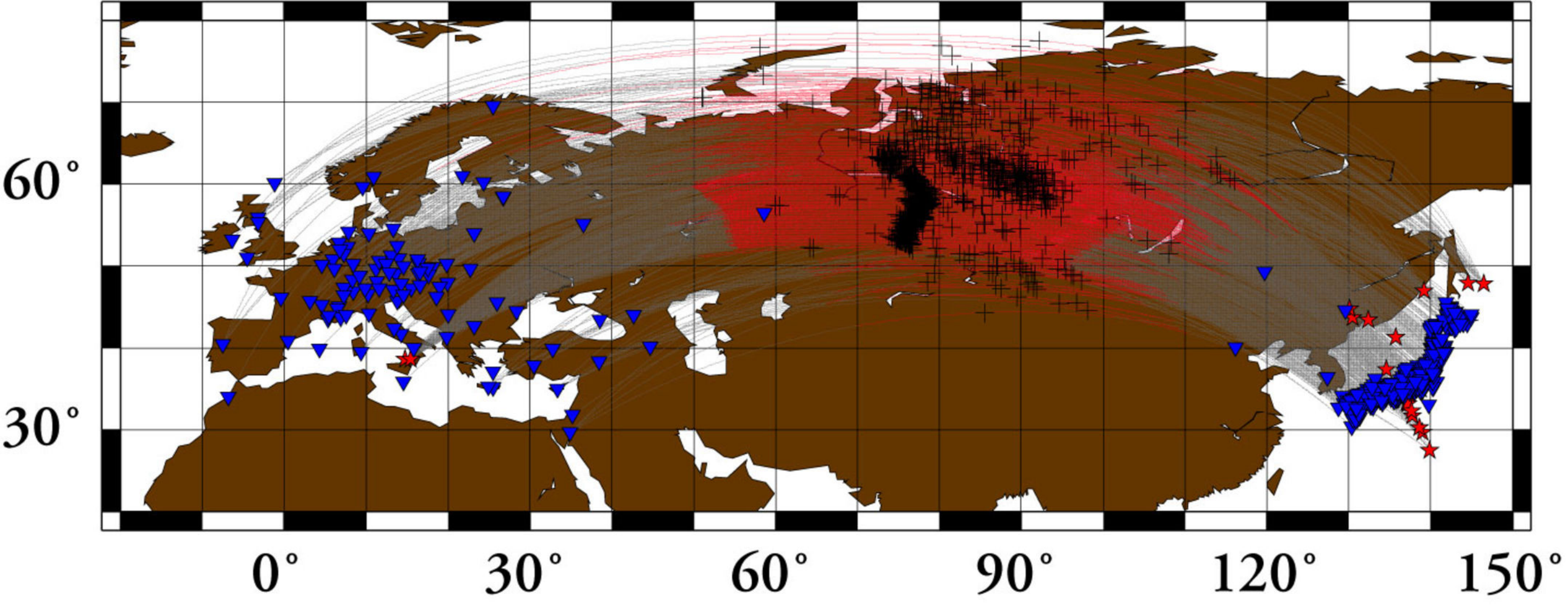
60°
30°
0°
30°
60°
90°
120°
150°

(a)

(b)

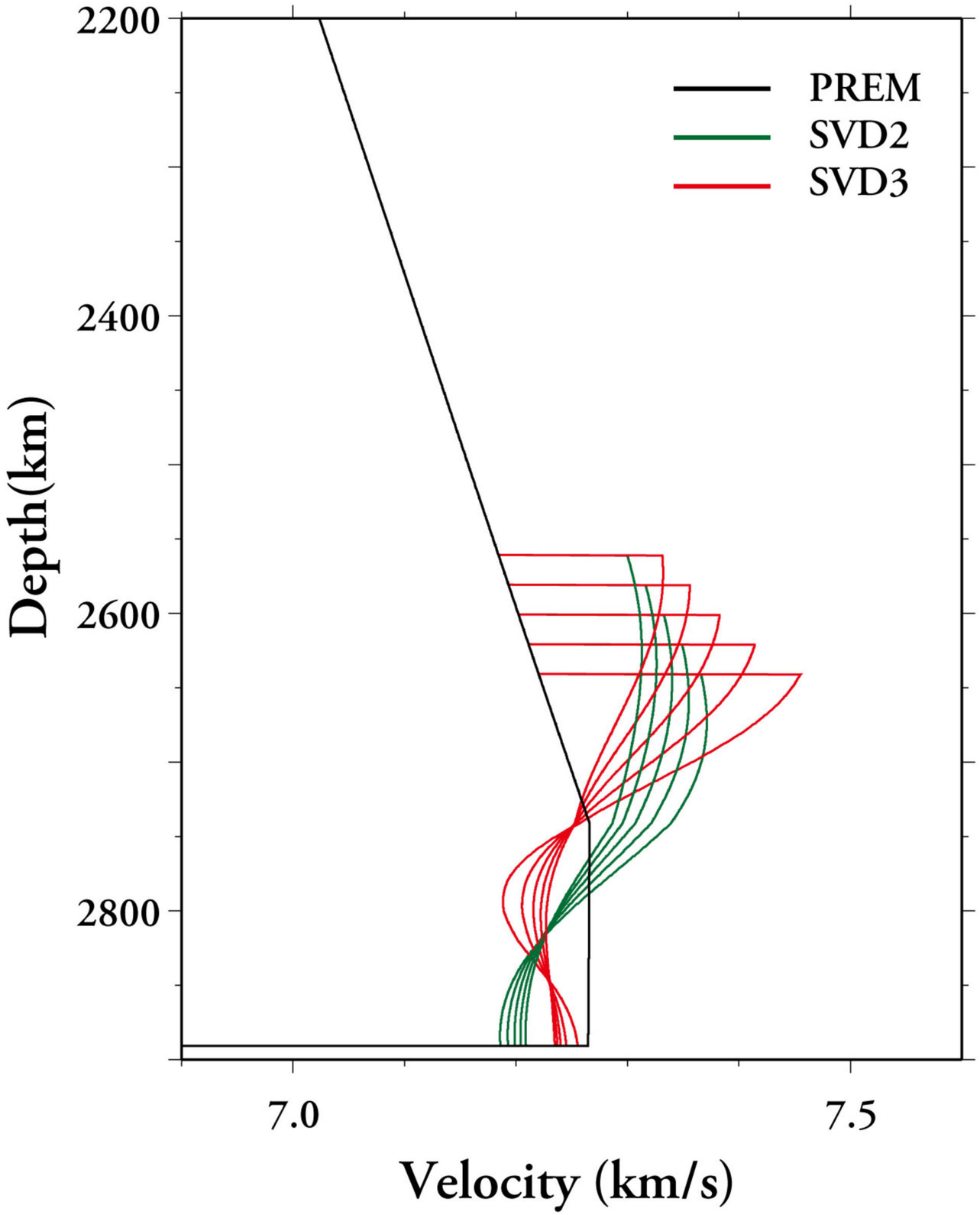
2200
2400
2600
2800
Depth(km)
PREM
SVD2
SVD3
7.0
7.5
Velocity (km/s)

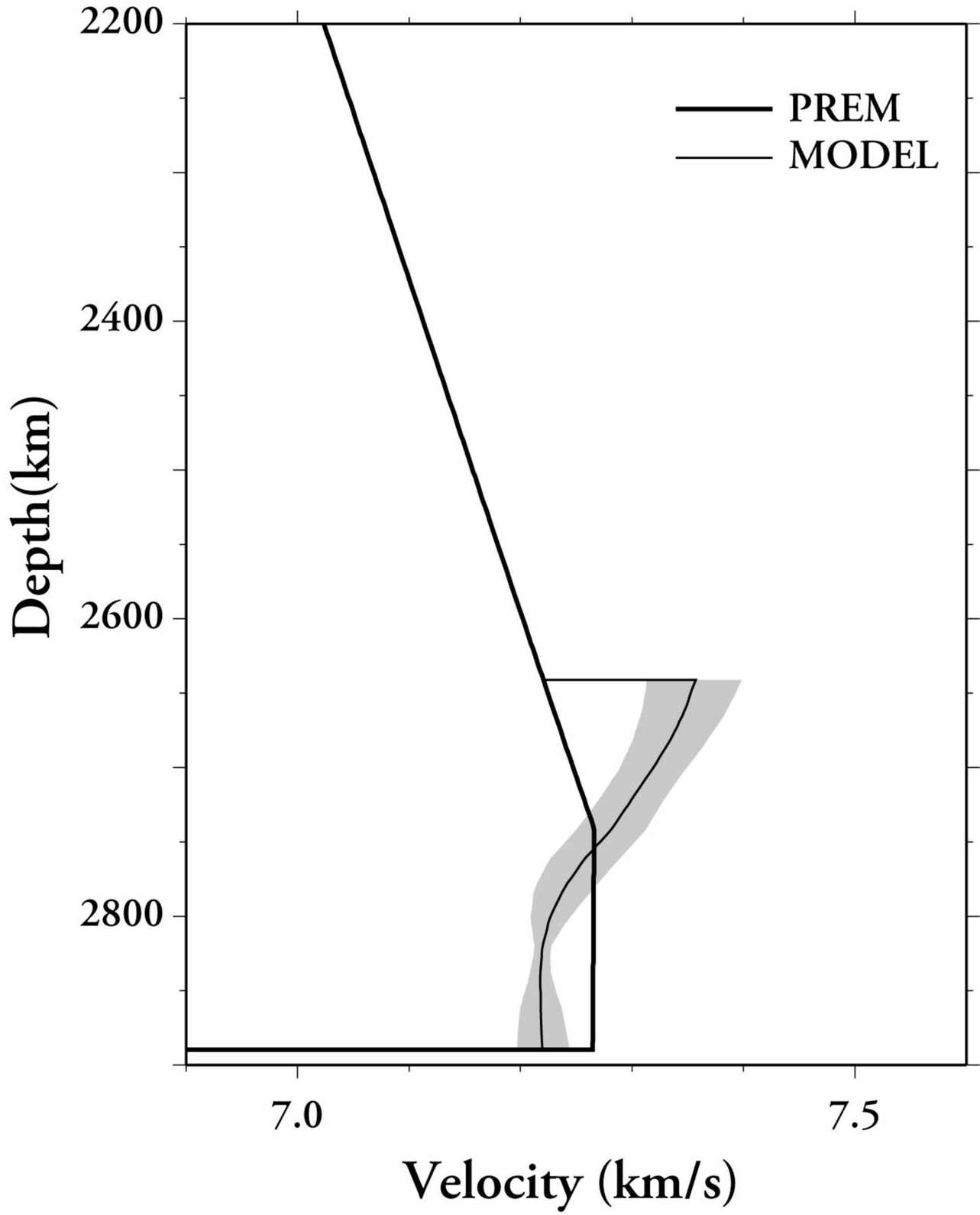
2200
2400
2600
2800
Depth(km)
PREM
MODEL
7.0
7.5
Velocity (km/s)

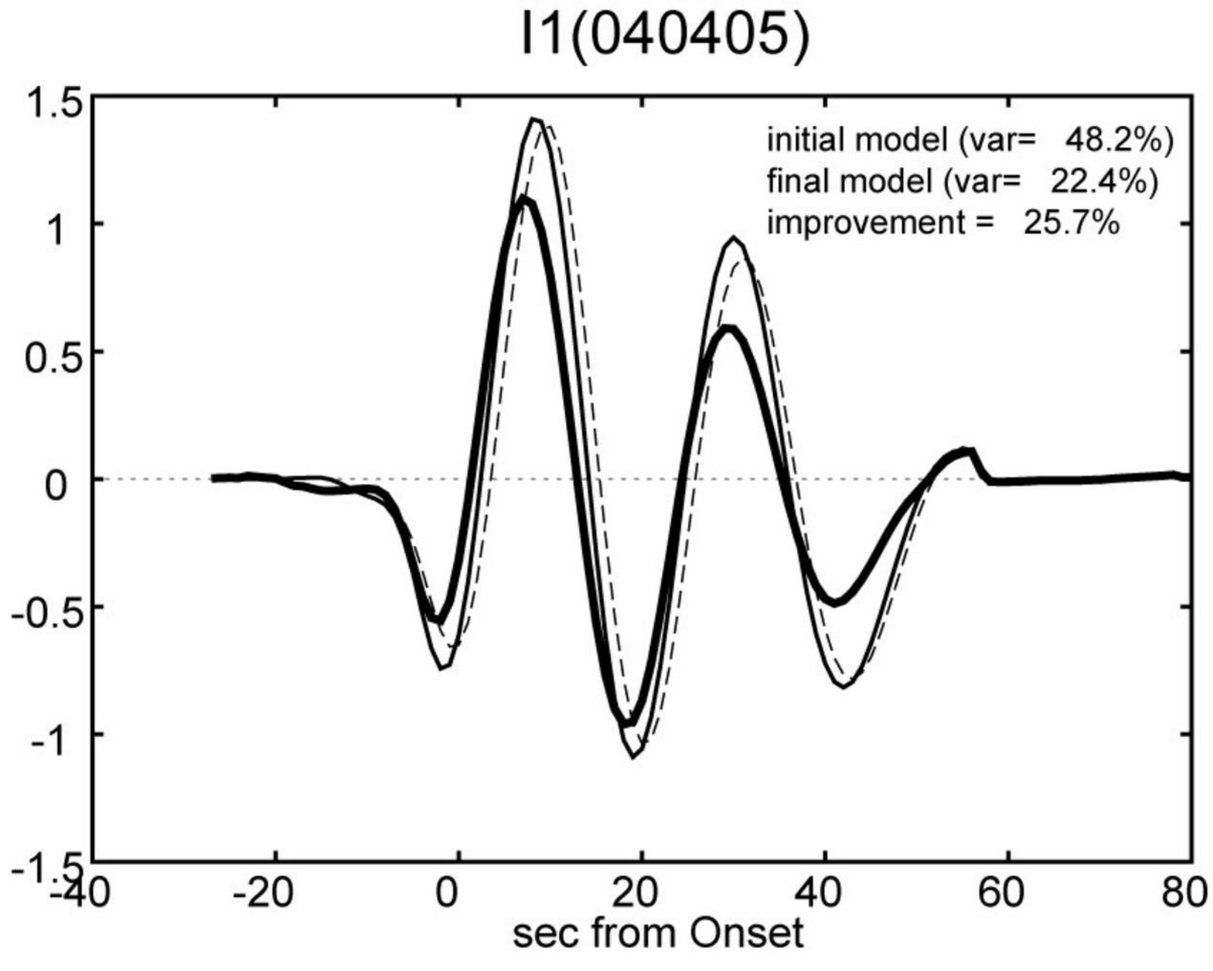
I1(040405)
initial model (var= 48.2%)
final model (var= 22.4%)
improvement = 25.7%
sec from Onset

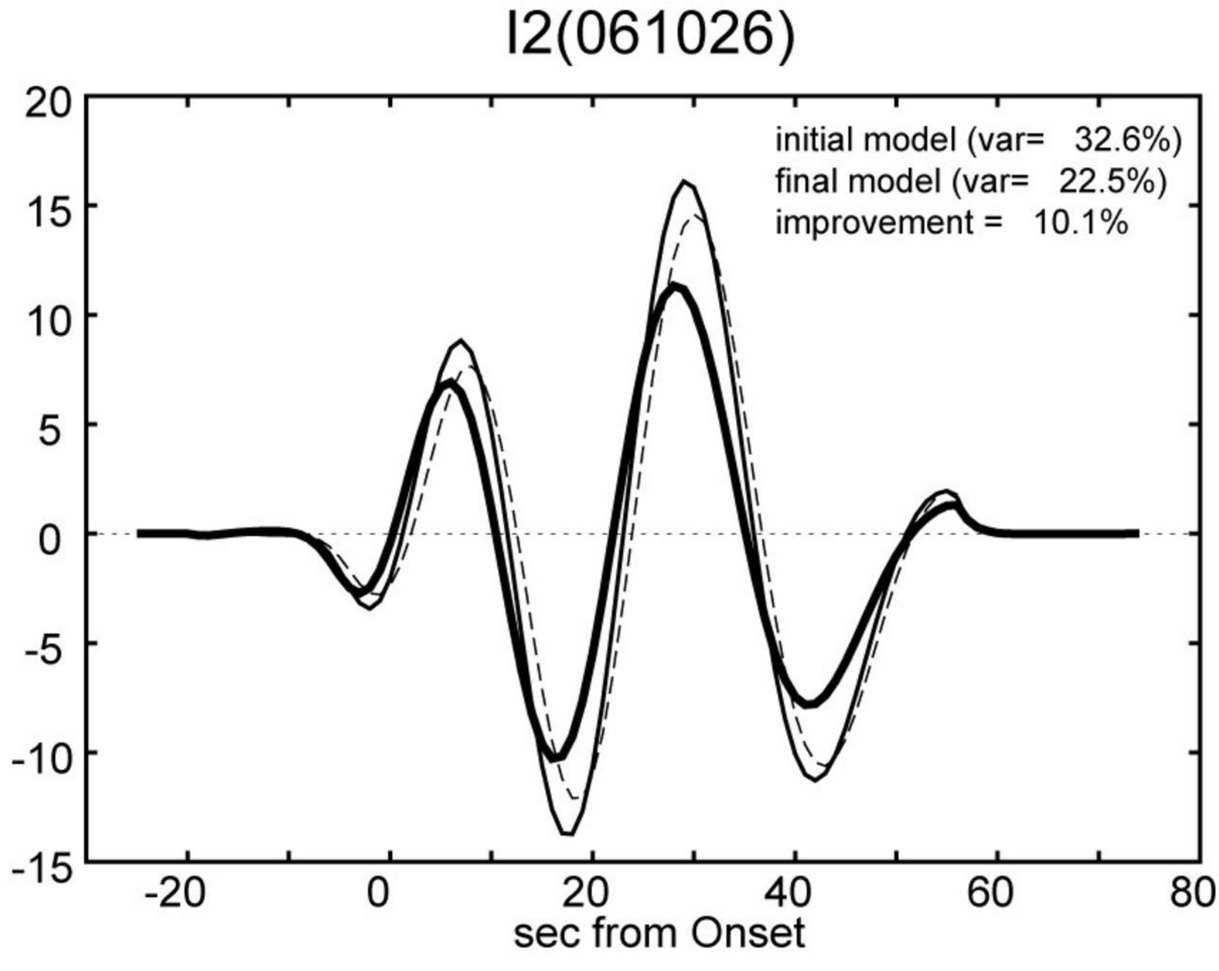
I2(061026)
initial model (var= 32.6%)
final model (var= 22.5%)
improvement = 10.1%
sec from Onset

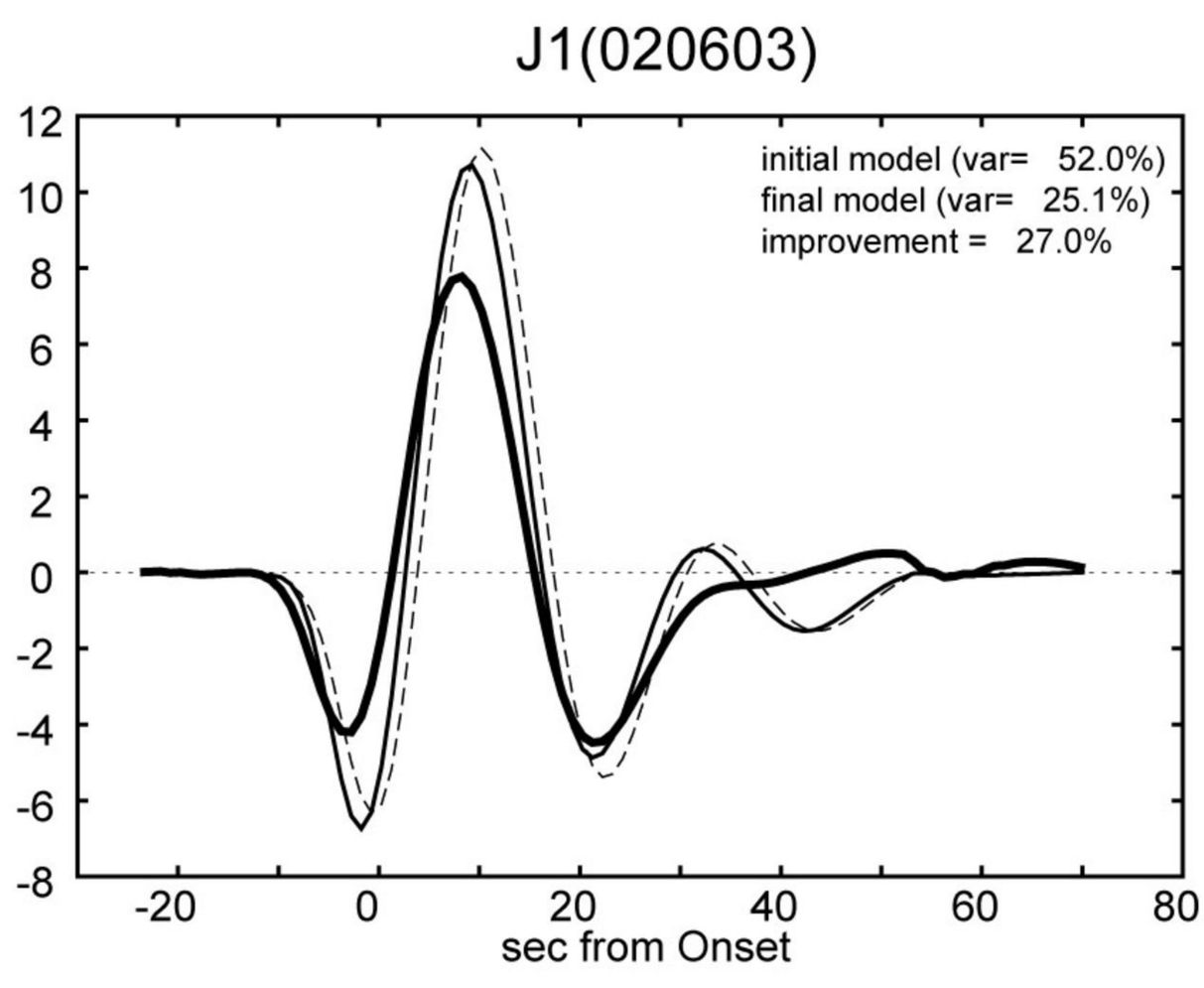
J1(020603)
initial model (var= 52.0%)
final model (var= 25.1%)
improvement = 27.0%
sec from Onset

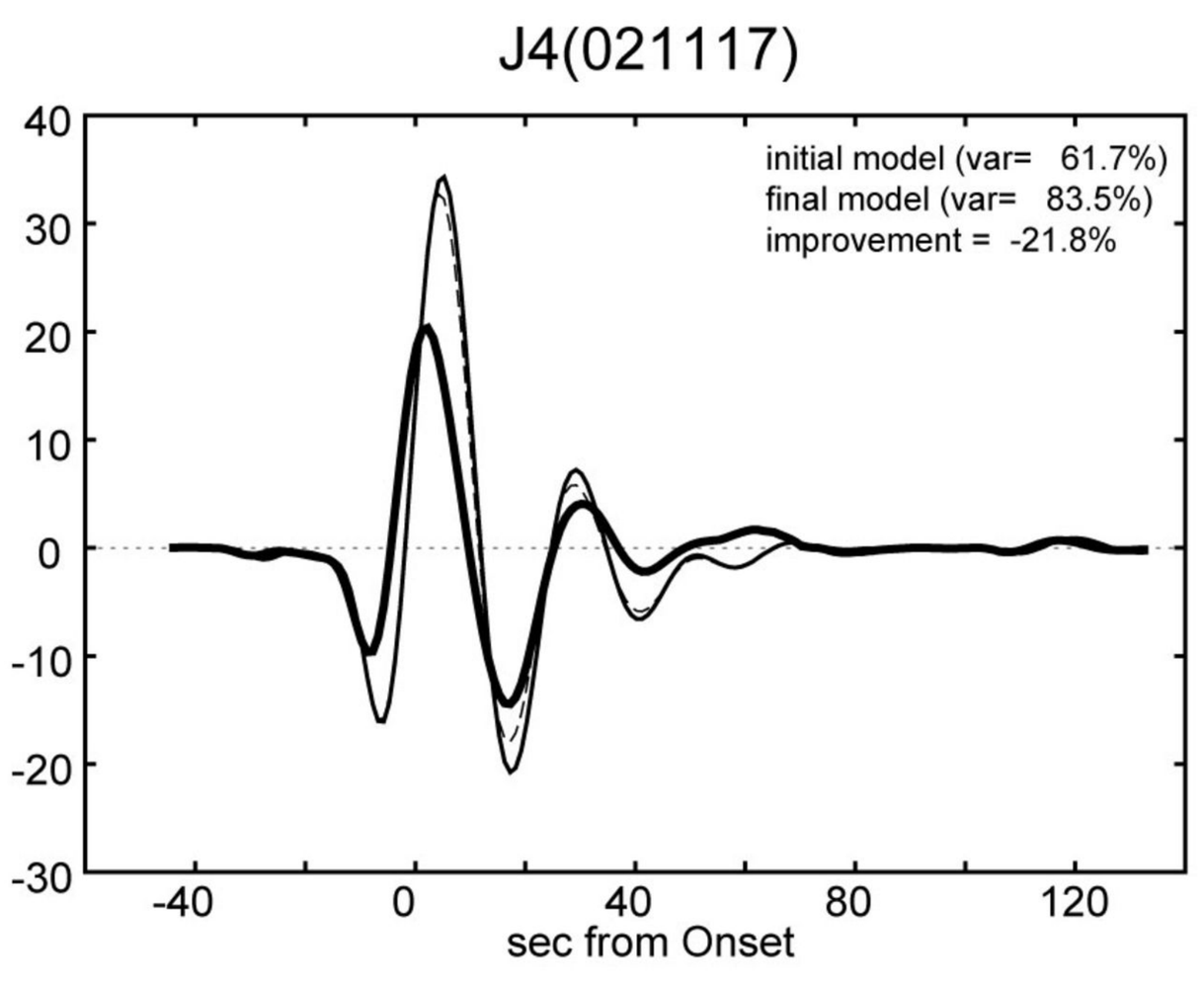
J4(021117)
initial model (var= 61.7%)
final model (var= 83.5%)
improvement = -21.8%
sec from Onset

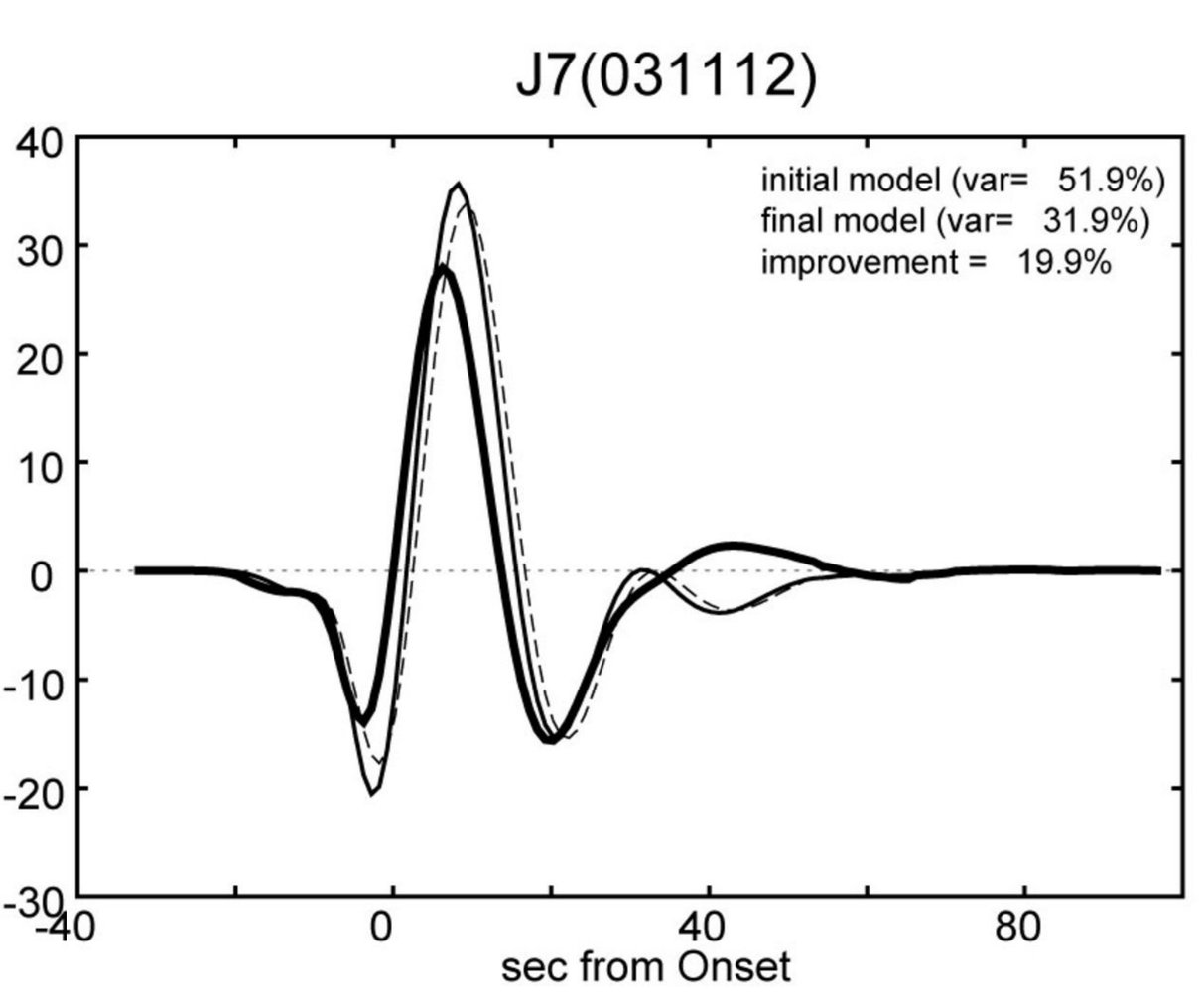
J7(031112)
initial model (var= 51.9%)
final model (var= 31.9%)
improvement = 19.9%
sec from Onset

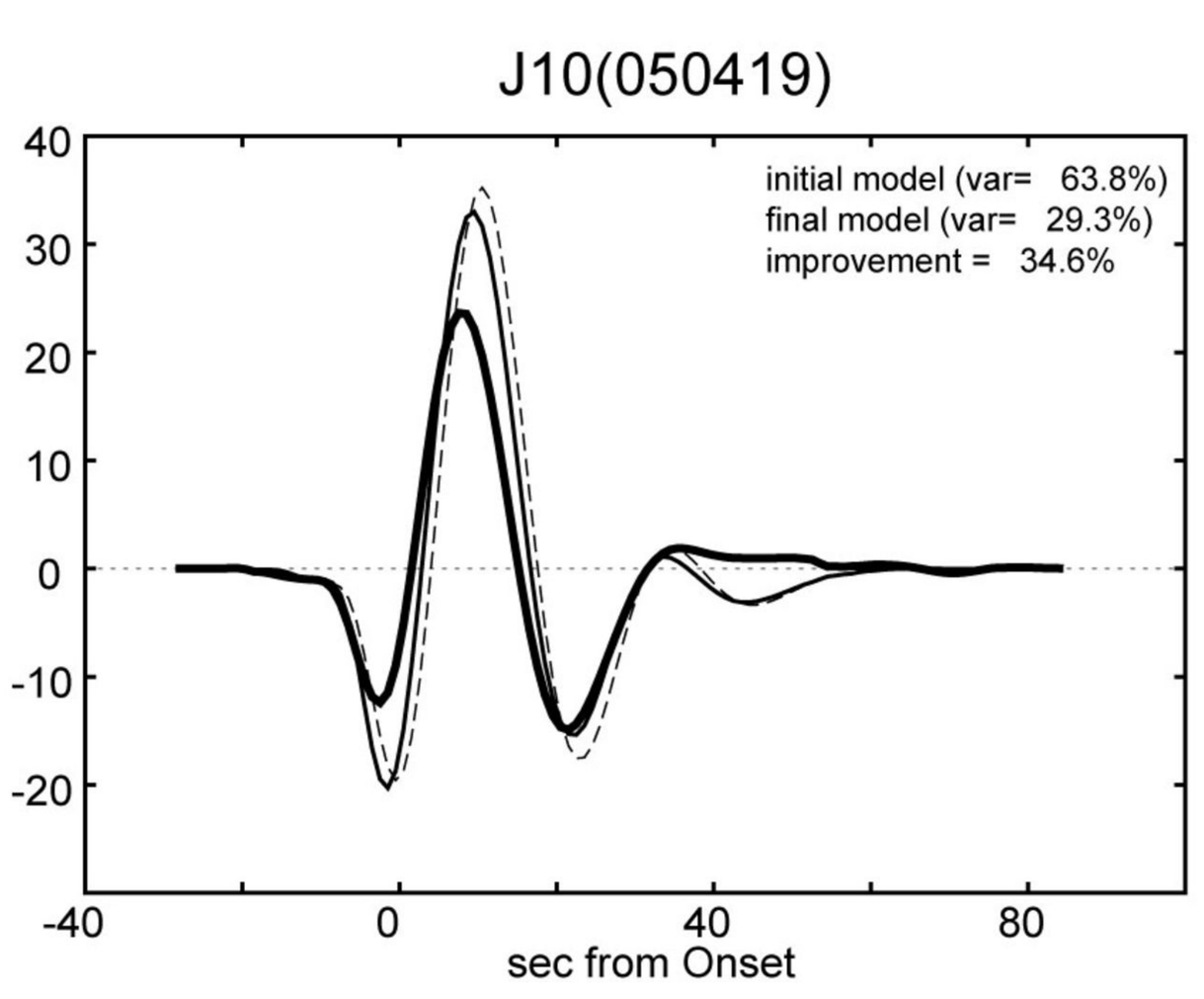
J10(050419)
initial model (var= 63.8%)
final model (var= 29.3%)
improvement = 34.6%
sec from Onset

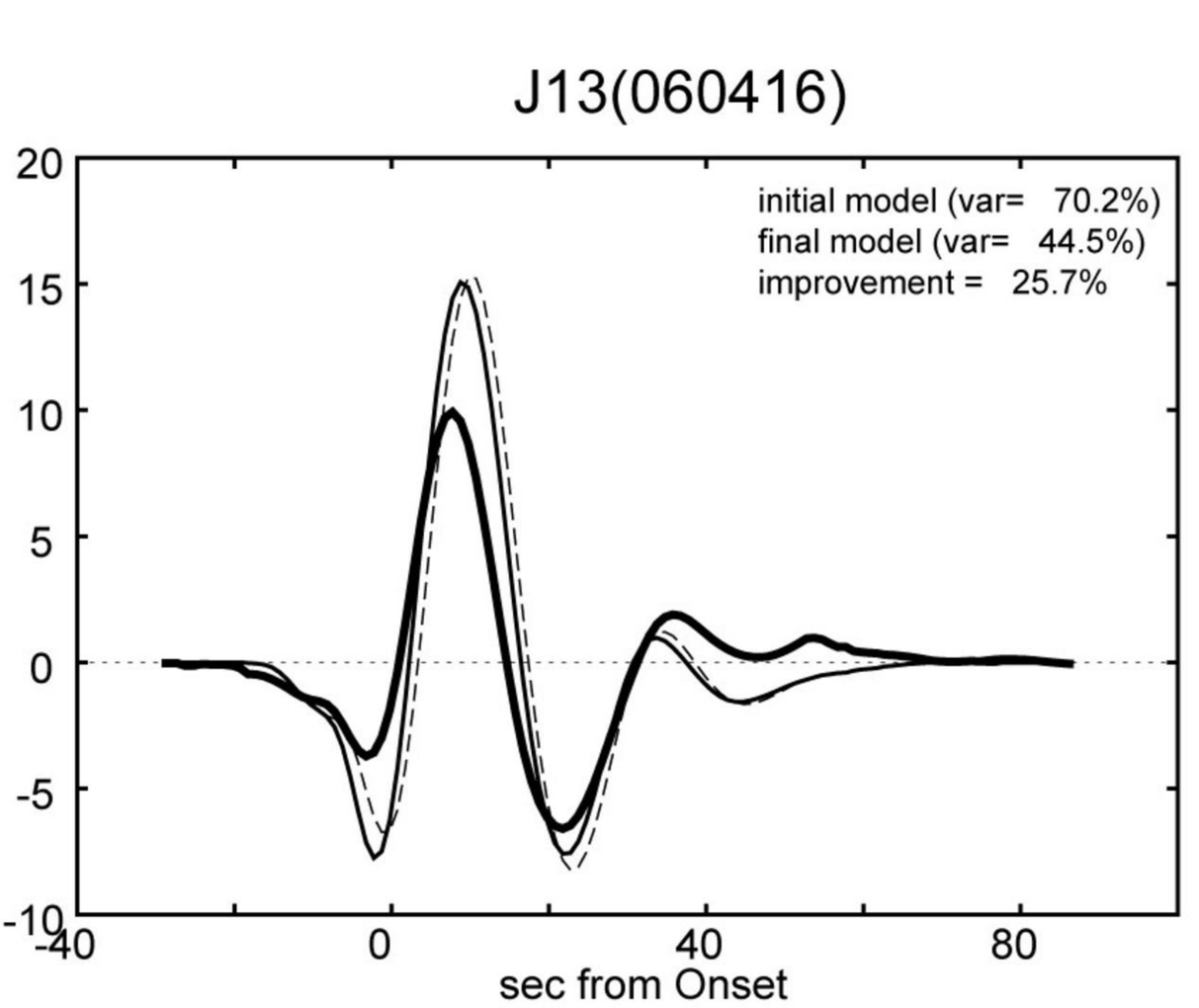
J13(060416)
initial model (var= 70.2%)
final model (var= 44.5%)
improvement = 25.7%
sec from Onset

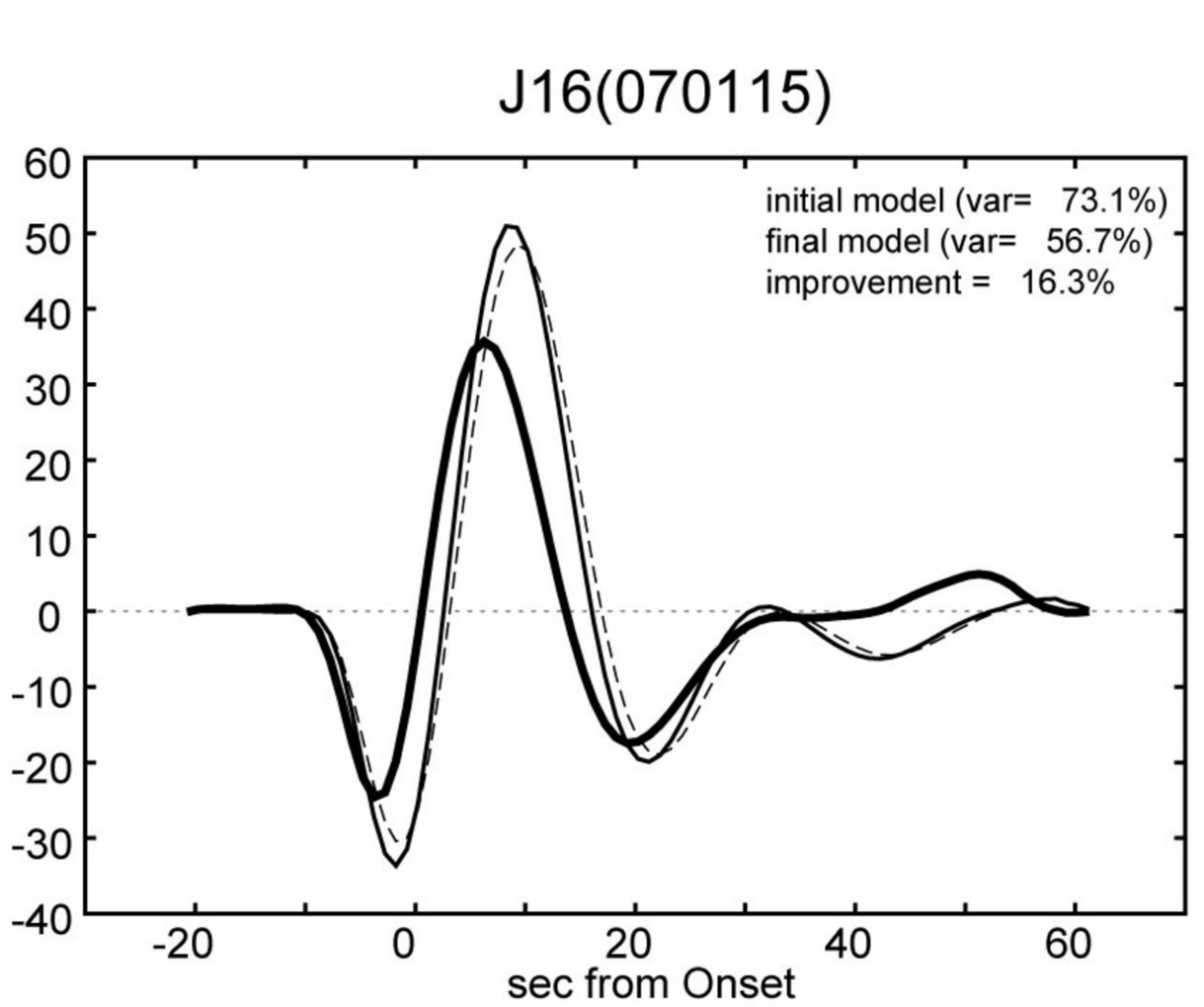
J16(070115)
initial model (var= 73.1%)
final model (var= 56.7%)
improvement = 16.3%
sec from Onset

(a)

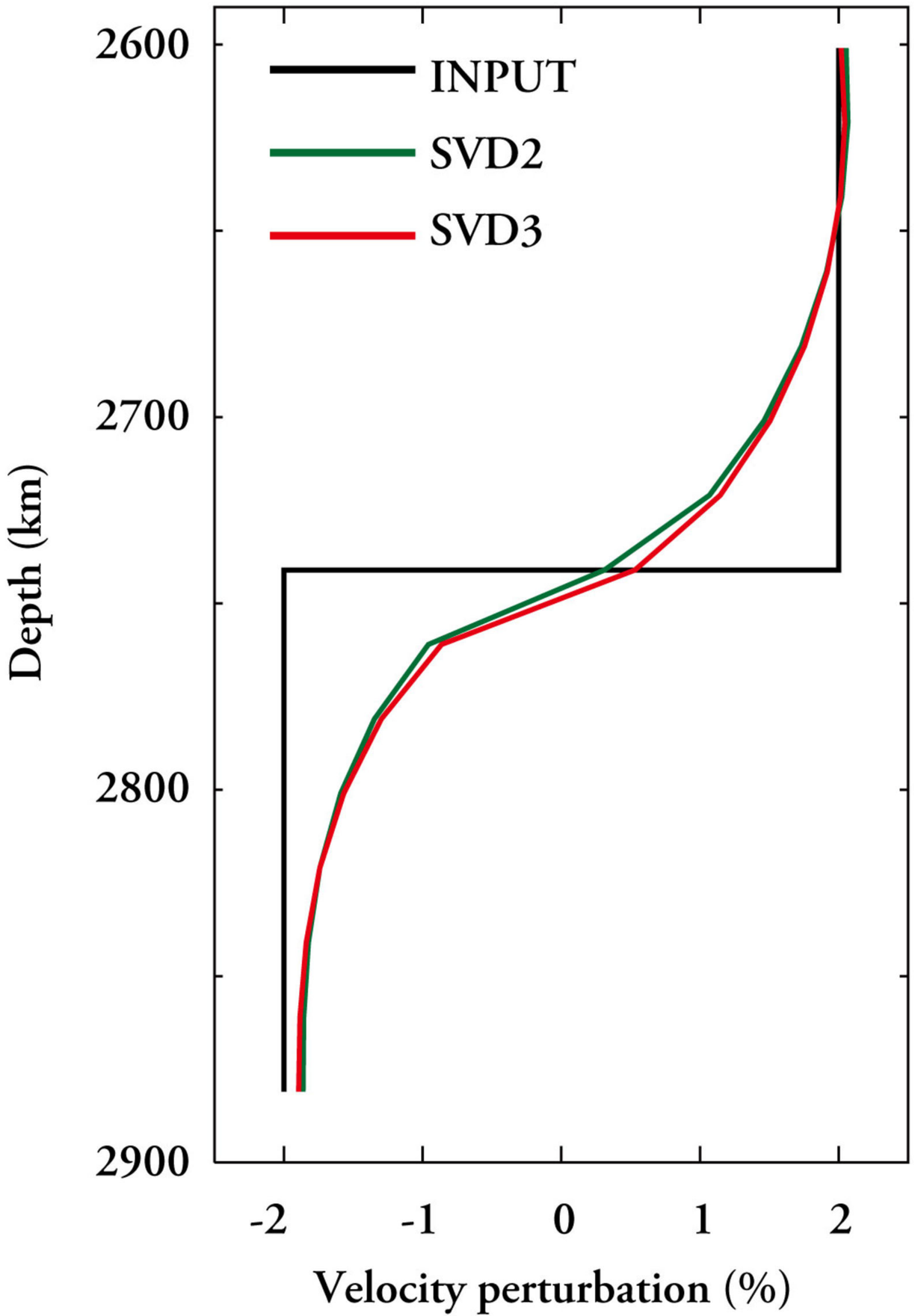
2600
2700
2800
2900
Depth (km)
INPUT
SVD2
SVD3
-2
-1
0
1
2
Velocity perturbation (%)

(b)

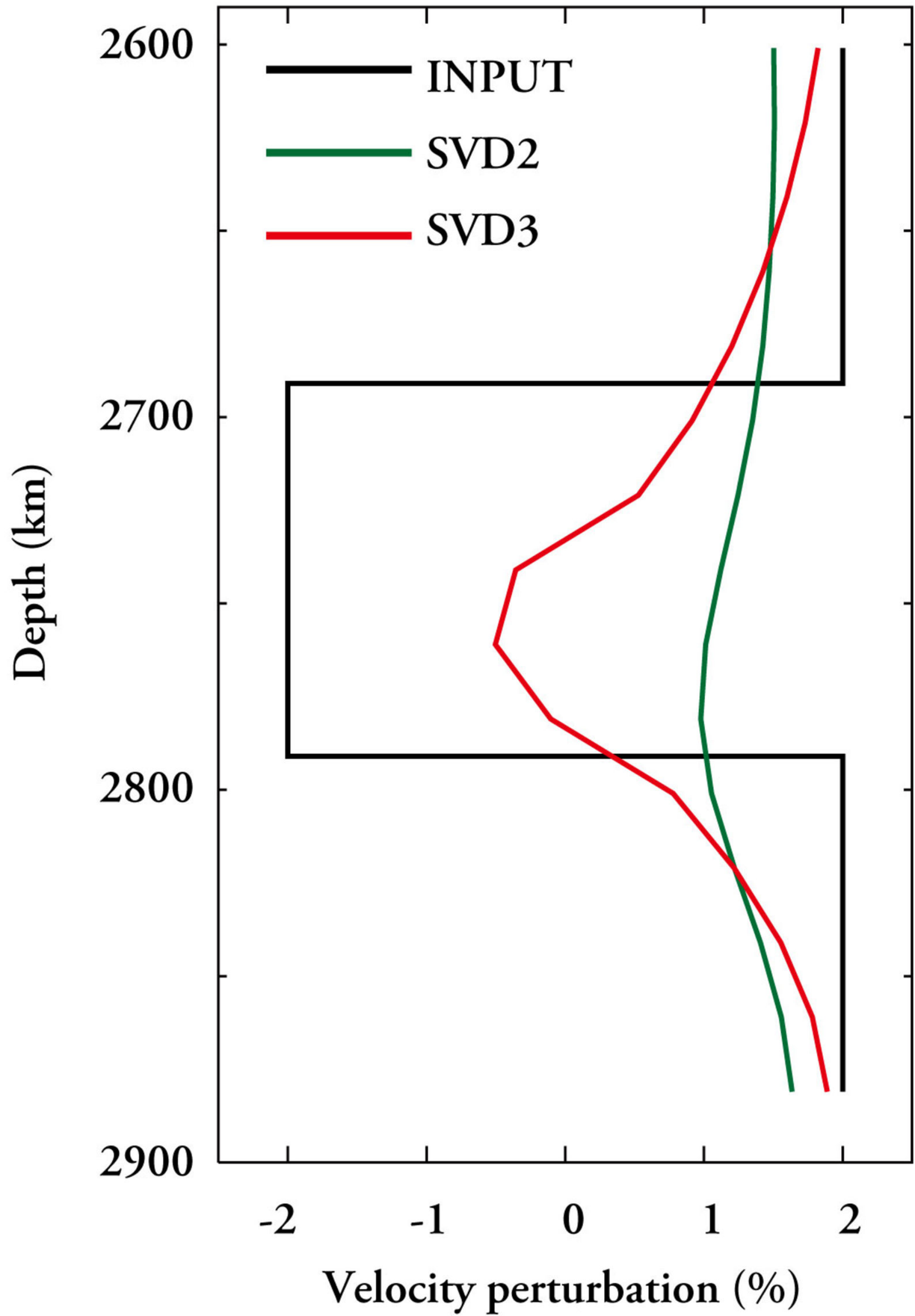
2600
2700
2800
2900
Depth (km)
INPUT
SVD2
SVD3
-2
-1
0
1
2
Velocity perturbation (%)